ACADEMIC CERTIFICATE AND TRANSCRIPT

OFFICE OF THE REGISTRAR

CHULALONGKORN UNIVERSITY

Bangkok 10330, Thailand

No. 602180/2563

THIS IS TO CERTIFY THAT

Mr. Kit Janprasit

Student ID   607 04310 21   **Identification No.**   1 7497 00000 07 1

has completed all the requirements for the Master of Engineering Degree

field of study Civil Engineering.

The University Council admitted the Master of Engineering Degree on January 17, 2020.

Given on January 31, 2020

Mana Si

(Assoc. Prof. Dr. Mana Sriyudthsak)

Registrar

NOT VALID WITHOUT UNIVERSITY SEAL

You can download CU DOCVERIFY application from Appstore and Playstore to validate the documents.

1300542351307

Mahidol University

Confers

The Degree of Bachelor of Engineering
(Civil Engineering)

Upon

Kit Janprasit

Who has passed the required examination

With all the Honors, Rights and Privileges thereto pertaining given this on

February 14, 2018

Vice-Chairman for Chairman of the University Council

Acting President

Dean
Faculty of Engineering

AUTODESK

Jun 22, 2022

Kit Janprasit

has successfully completed

Autodesk Certified Professional: Revit for Structural Design Exam Prep

an online non-credit course authorized by Autodesk and offered through Coursera

Andrew Anagnost, President and Chief Executive Officer of Autodesk, Inc.

EDUCATION FOR EVERYONE · **coursera** · COURSE CERTIFICATE

coursera
project
network

COURSE CERTIFICATE

Jul 23, 2021

Kit Janprasit

has successfully completed

Stock Valuation with Comparable Companies Analysis

an online non-credit course authorized by Coursera Project Network and offered through Coursera
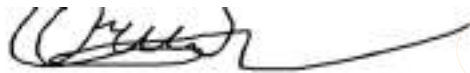
Bekhruzbek Ochilov, ACSI
Investment Analyst

EDUCATION FOR EVERYONE · coursera · COURSE CERTIFICATE

PUBLISHED PAPER

Enhancement of strengths of high-calcium fly ash geopolymer containing borax with rice husk ash

Peem Nuaklong, Kit Janprasit, Pitcha Jongvivatsakul *

Innovative Construction Materials Research Unit, Department of Civil Engineering, Faculty of Engineering, Chulalongkorn University, Bangkok, 10330, Thailand

ARTICLE INFO

ABSTRACT

The objective of this study was to investigate the microstructure and mechanical properties of a high-calcium fly ash geopolymer prepared with borax modified by the addition of rice husk ash (RHA). The sodium silicate was replaced with borax, on an equal mass basis, at 0, 10, 20, and 30%. The results showed that the use of borax instead of sodium silicate reduced both the compressive and flexural strengths. The strength decreases when borax was used were related to the increase in the crystalline nature of the reaction products caused by the decreases in the Si/Al ratios of the gel phases formed. Moreover, incorporating 3.6–6.0% RHA into geopolymer mortars containing either hydrated borax or anhydrous borax led to an improvement in the compressive strength due to the formation of a Ca-modified N-A-S-H gel with a high Si/Al ratio during the reaction.

1. Introduction

The growing concern over global climate change is forcing researchers to pay attention to the development of inorganic polymer cements or "geopolymers." Geopolymers are attractive because of their potential to reduce CO_2 emissions compared to Portland cements [1–3]. In addition, the use of geopolymers for construction materials will address waste management issues, such as by reducing the waste placed in landfills and improving waste utilization [4,5]. Waste materials such as fly ash, blast furnace slag and sludge can be used as geopolymer precursors [6–10]. The cementitious properties of geopolymers develop because of reactions between the precursor compounds and alkali activators. Among the activators, sodium silicate and sodium hydroxide are widely used [1]. However, they are the causes of environmental and other problems with geopolymer binders, especially the production of sodium silicate [11]. Its manufacturing processes involve burning quartz sand and sodium carbonate at temperatures of 1,400–1,500 °C, which can affect the environment in the form of harmful gaseous CO_2 [12,13]. Therefore, new activators are needed to replace the common sources for enhanced environmental performance.

Attempts to produce a more environmentally friendly type of geopolymer cement have resulted in the development of boroaluminosilicate geopolymers, which develop high strength from the formation of the B–O bond [6,14,15]. Borax has been promoted as an activator for geopolymer cement in order to decrease the consumption of sodium silicate. It is considered relatively clean compared with common silicate compounds; in addition, the advantages of using borax would include the human safety and the decreased cost of geopolymers [16]. In addition, Bagheri et al. [14] suggested that the reduction in strength due to the decrease in the dosage of sodium silicate can be partly compensated by the incorporation of borax. To be effective, the borax content had to replace at least 10% of the sodium silicate by mass, and preferably 30% [14,15]. However, the combination of borax and sodium silicate produced a lower strength than is found in composites made from sodium silicate alone. Thus, the next step was to find an economical material that improved the strength of the geopolymer and could be collected from local suppliers and manufacturers.

In developing countries such as Thailand, agricultural residues are used as biofuels for energy production in biomass thermal power plants [17,18]. Among them, rice husk is quite attractive because it is abundant in agricultural waste and a large amount is available [17]. Rice husk is a by-product of the rice milling process and is usually burned for various heating purposes [19]. Although biomass energy resources are cleaner than fossil fuels [20], it is well known that burning rice husk leaves behind solid waste, called rice husk ash (RHA), which needs to be properly disposed of to avoid adverse environmental effects. Fortunately, burning rice husks results in the formation of silica (SiO_2) in the RHA [21]. While crystalline SiO_2 is suggested for producing products such as refractory bricks and ceramics, the amorphous and hydrated phases are useful as additive materials in the cement industry [17,22,

Table 1
Properties of high-calcium fly ash and RHA.

Composition (%)	Fly ash	RHA
Chemical composition		
SiO_2	31.5	81.6
Al_2O_3	18.6	–
CaO	18.6	1.7
Fe_2O_3	14.8	6.5
MgO	2.7	0.9
K_2O	2.1	8.9
Na_2O	2.3	–
TiO_2	0.4	–
P_2O_5	0.3	–
SO_3	4.6	0.2
Physical properties		
Specific gravity	2.3	2.1
BET specific surface area (m^2/g)	4.6	16.3
Median particle size (μm)	16.4	13.9
LOI (%)	0.6	2.3

23]. Therefore, dumping RHA into landfills or open fields may become unnecessary.

Numerous reports on the properties of geopolymers made from RHA have been published [24–27]. The inclusion of RHA, at an optimum dosage, was found to increase the compressive strength of geopolymer paste [25], partly because of the higher density of Si–O–Si linkages, which are stronger than those of Si–O–Al and Al–*O*–Al bonds [28]. In addition, previous studies reported that the compressive strengths of geopolymer concretes could be improved by incorporating RHA into the mixtures [24]. It was also found that the effectiveness of RHA in improving the strength of geopolymer concrete was comparable to that of nano-silica [26]. However, research on the use of RHA to enhance the performance of geopolymers containing borax has not been reported.

The objective of this study was to experimentally investigate the effect of RHA on the properties of high-calcium fly ash geopolymers manufactured using hydrated borax and anhydrous borax. A total of 25 mortar mixtures were cast, and their compressive and flexural strengths were tested. Two types of borax were utilized, namely hydrated borax and anhydrous borax. The specimens with borax were produced by the partial substitution of sodium silicate with borax at varying amounts of 10–30%. The rice husk ash was used as an additive material to enhance the performance of geopolymers containing borax. Therefore, RHA were added at 3.6%, 4.8%, and 6.0% by weight of fly ash, while the fly ash content was kept constant. Moreover, the microstructures of the geopolymer pastes were evaluated for the purpose of understanding their influence on the strength behavior of the mortar.

2. Materials and methods

2.1. Materials

High-calcium fly ash with a specific gravity of 2.3 was used as the primary precursor. It was obtained from a coal-fired power station in Lampang, Thailand. The RHA used in the present work was ground for 8 h to obtain a BET specific surface area of 16.3 m^2/g. Table 1 presents the chemical composition, as determined by X-ray fluorescence (XRF) spectrometry. The main components of the fly ash were SiO_2, Al_2O_3, CaO, and Fe_2O_3, while the major oxide of the RHA was SiO_2.

The common alkali activators used were a 10 M sodium hydroxide solution (NH) and a sodium silicate solution (NS) with 30.0% SiO_2, 14.5% Na_2O, and 55.3% H_2O. In this study, two forms of borax were used as an alternative to sodium silicate: borax decahydrate ($Na_2B_4O_7 \cdot 10H_2O$) and anhydrous borax ($Na_2B_4O_7$). The latter was produced by heating borax decahydrate at 150 °C for 30 min and then at 300 °C for 15 h [6,15,16,29,30].

The fine aggregate used for making the geopolymer mortars was river sand with a gradation meeting ASTM standard C33 [31] (Fig. 1). The grading of the aggregate was determined using a sieve analysis
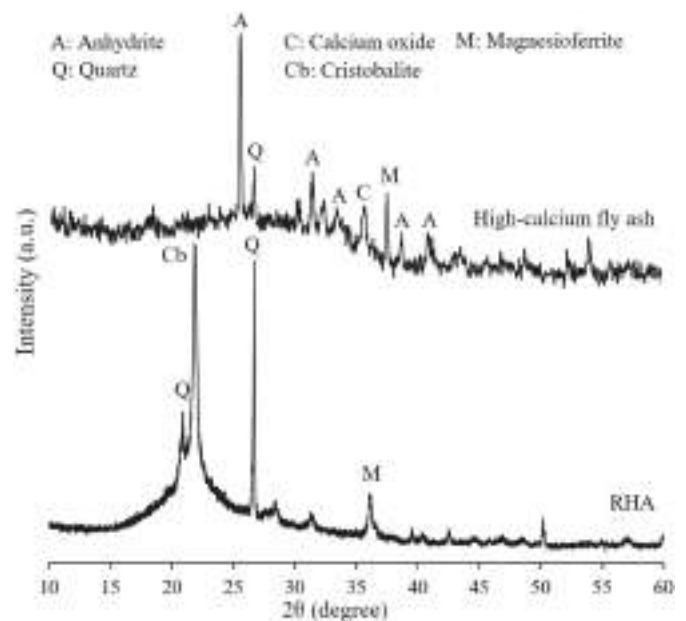
Fig. 2. XRD patterns of high-calcium fly ash and RHA.
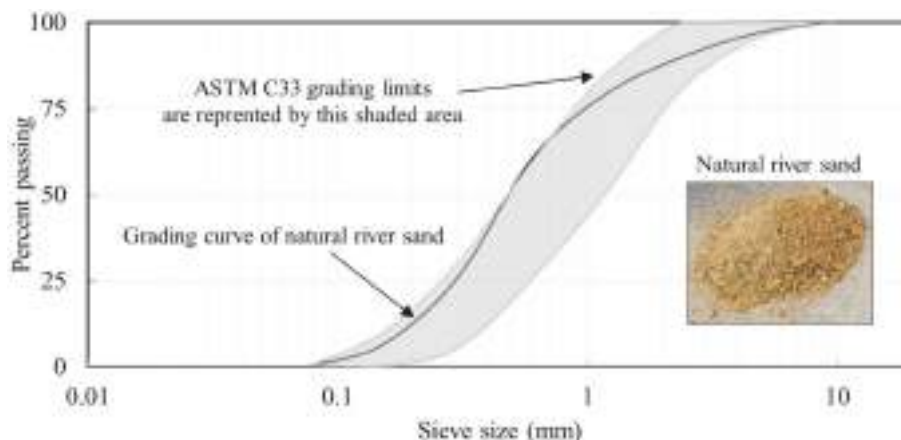
Fig. 1. Grading curve of natural river sand used in investigation.
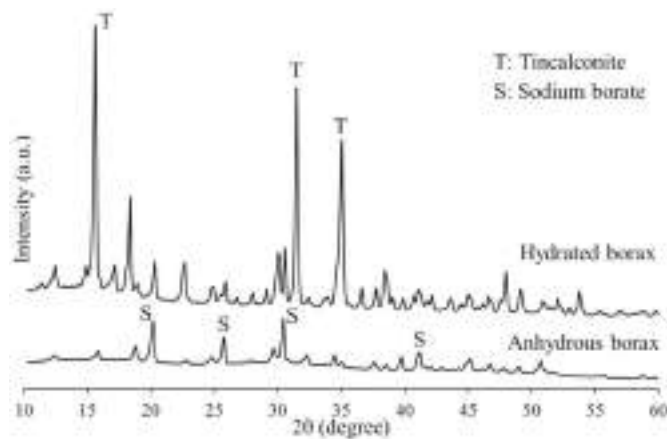
Fig. 3. XRD patterns of hydrated borax and anhydrous borax.

following ASTM C136 [32]. A fineness modulus of 2.42 was computed from the sieve analysis data. The aggregate had specific gravity and water absorption values of 2.57 and 0.72%, respectively. These values were determined using the methods outlined in ASTM C128 [33]. The dry-rodded unit weight of the aggregate used in the study was 1,639 kg/m^3, which was determined in accordance with ASTM C29 [34].

The X-ray diffraction (XRD) patterns of the fly ash and RHA are shown in Fig. 2. The results showed that the fly ash was mainly glassy; moreover, crystalline phases of anhydrite ($CaSO_4$), quartz (SiO_2), lime (CaO), and magnesioferrite ($MgFe_2O_4$) were detected in the XRD pattern. The RHA contained amorphous silica with crystalline inclusions of cristobalite (SiO_2), quartz, and magnesioferrite.

Fig. 3 illustrates the XRD patterns of the hydrated borax and anhydrous borax used in the investigation. The hydrated borax exhibited the high-intensity crystalline peaks of tincalconite ($Na_2B_4O_7 \cdot 5H_2O$). The results also indicated that the anhydrous borax showed a lower degree of crystallinity compared to the hydrated borax. After heating, no sharp peaks of tincalconite at 2θ values of 15.63°, 31.49°, and 35.06° were found in the XRD pattern for the anhydrous borax. In addition,

Waclawska [35] suggested that an amorphous sodium borate was the main product of dehydration. These results indicated that the anhydrous borax was more reactive than the hydrated borax. However, the crystalline peaks of sodium borate were also observed in the diffraction pattern.

2.2. Mix proportions

The mix proportions of the mortar specimens are listed in Table 2. All the geopolymer mortars were made with an activator-to-fly ash mass ratio of 0.6. In addition, they were proportioned to have an (NS + borax)-to-NH ratio of 0.5. The mass ratio of fly ash to sand was kept constant at 1:2.75 for all the mixtures. Based on these proportions, the workable flow of the control mortar was in the range of 110 ± 5%, which met the requirements of ASTM C109 [36].

The mix variables included the type of borax, amount of borax as a replacement for NS, and amount of RHA. In addition to reducing the consumption of NS, the current study attempted to promote the use of hydrated borax instead of anhydrous borax as an activator for geopolymer composites. The labels "H" and "A" indicate that the mixtures were prepared using hydrated borax or anhydrous borax, respectively. Borax was used as a replacement for the NS at 0, 10, 20, and 30% by weight. In order to improve the performance of the geopolymer composites made with borax, small quantities of RHA particles (3.6%, 4.8%, and 6.0% by mass of fly ash) were added to the mixtures.

2.3. Specimen preparation

The procedure for mixing the geopolymer mortar was as follows. First, fly ash and RHA were manually dry mixed before mixing with the other ingredients. Second, the dry materials (fly ash and RHA) and NH were poured into a mortar mixer and mixed continuously for 5 min. Third, river sand in a saturated surface dry condition was added to the rotating mixer. Finally, NS and borax were added after mixing for 10 min, and the mixing was continued for a further 5 min.

The geopolymer paste had similar mix proportions to the mortar except the river sand was absent in the paste. The mixing time for the paste used in the current study was approximately 10 min. The dry

Table 2
Proportions of geopolymer mortar mixtures.

Mix	Borax (%)	RHA (%)	Mix proportions (g)						
			Fly ash	RHA	NH	NS	Hydrated borax	Anhydrous borax	River sand
Control	0	0	100	–	40	20	–	–	275
10H	10	0	100	–	40	18	2	–	275
20H	20	0	100	–	40	16	4	–	275
30H	30	0	100	–	40	14	6	–	275
10H-3.6	10	3.6	100	3.6	40	18	2	–	275
20H-3.6	20	3.6	100	3.6	40	16	4	–	275
30H-3.6	30	3.6	100	3.6	40	14	6	–	275
10H-4.8	10	4.8	100	4.8	40	18	2	–	275
20H-4.8	20	4.8	100	4.8	40	16	4	–	275
30H-4.8	30	4.8	100	4.8	40	14	6	–	275
10H-6.0	10	6.0	100	6.0	40	18	2	–	275
20H-6.0	20	6.0	100	6.0	40	16	4	–	275
30H-6.0	30	6.0	100	6.0	40	14	6	–	275
10A	10	0	100	–	40	18	–	2	275
20A	20	0	100	–	40	16	–	4	275
30A	30	0	100	–	40	14	–	6	275
10A-3.6	10	3.6	100	3.6	40	18	–	2	275
20A-3.6	20	3.6	100	3.6	40	16	–	4	275
30A-3.6	30	3.6	100	3.6	40	14	–	6	275
10A-4.8	10	4.8	100	4.8	40	18	–	2	275
20A-4.8	20	4.8	100	4.8	40	16	–	4	275
30A-4.8	30	4.8	100	4.8	40	14	–	6	275
10A-6.0	10	6.0	100	6.0	40	18	–	2	275
20A-6.0	20	6.0	100	6.0	40	16	–	4	275
30A-6.0	30	6.0	100	6.0	40	14	–	6	275
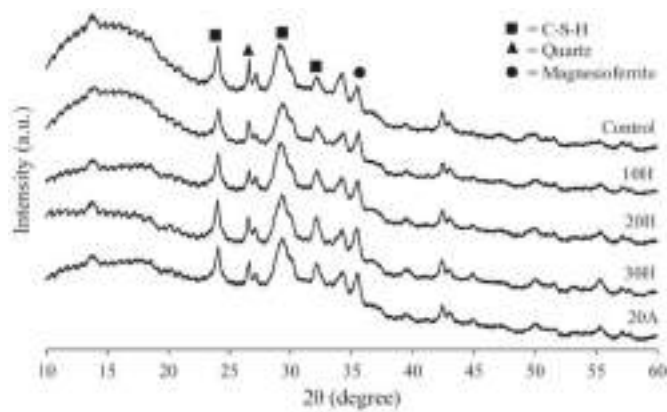
Fig. 4. Effects of borax replacement on phase compositions of geopolymers.
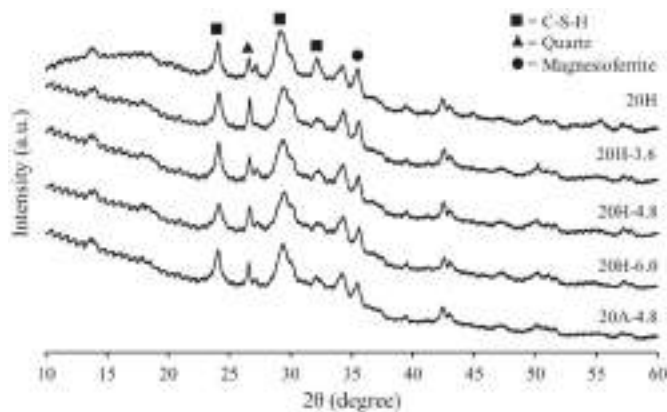
Fig. 5. Effects of RHA addition on phase compositions of geopolymers made with borax.

Fig. 6. FTIR results for geopolymers with different borax contents.

materials and NH were mixed in the mixer for 5 min before the final mixing with NS and borax. After mixing, the paste and mortar specimens were poured into molds and left at room temperature for 1 h, as suggested in previous publications [37–42]. Then, the specimens were cured in an oven for 24 h at 80 °C. After that, they were demolded and kept at room temperature until the age of 7 days.

2.4. Experimental study

The experimental study was divided into two parts: (1) a microstructural investigation of the geopolymer paste and (2) tests of the mortar properties. The microstructural observations consisted of XRD measurements, Fourier transform infrared spectroscopy (FTIR) analyses, and scanning electron microscopy (SEM)/energy dispersive spectroscopy (EDS) observations.

Microstructural studies are useful in understanding how the strength behaviors of geopolymers are associated with the presence of borax and RHA in the system. XRD was used to characterize the phase composition of each specimen. Before testing, the specimen was ground into powder form. Also, ground geopolymer specimens were analyzed using the FTIR-spectrum to determine the degree of geopolymerization. Broken geopolymer specimens were analyzed using the SEM technique to study their morphological characteristics. In addition, the detailed quantification of the hydrated paste was accomplished using EDS analysis.

The effects of borax and RHA on mechanical properties of the mortars were evaluated. The compressive strength and flexural strength were tested at the age of 7 days. To measure the compressive strength of the geopolymer mortar specimens, 50 × 50×50 mm³ cubic specimens were cast and tested according to the ASTM C109 [36]. The flexural
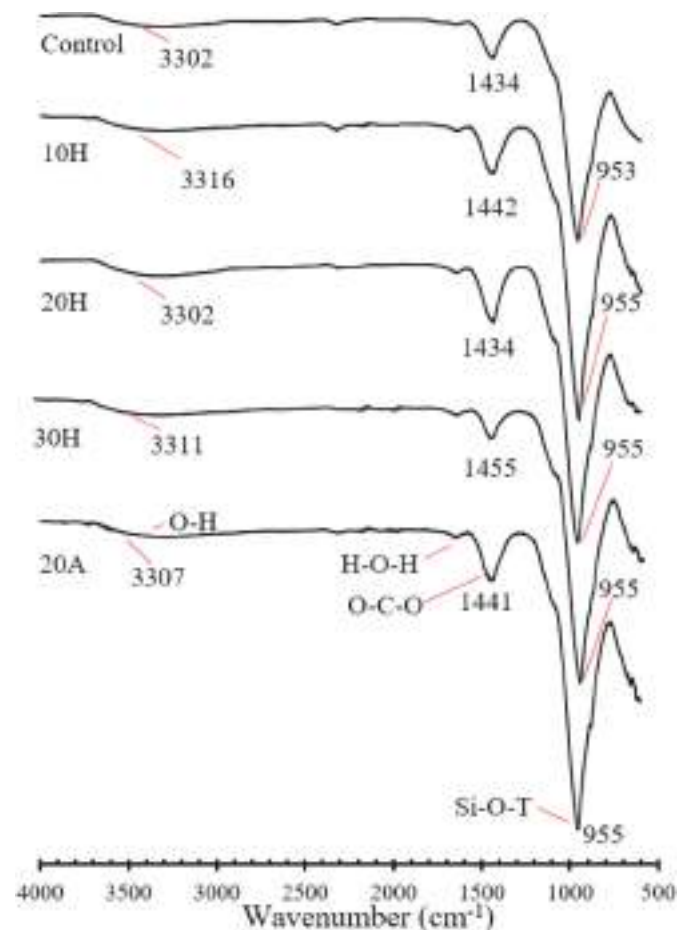
strength was measured using 40 × 40×160 mm³ beam specimens based on ASTM C348 [43]. It should be noted that each strength value was the average of those for three specimens.

3. Results and discussion

3.1. XRD patterns of geopolymer pastes

Figs. 4 and 5 show the diffraction patterns of the geopolymer specimens. It was found that the paste consisted mainly of aluminosilicate and calcium silicate compounds. The major crystalline phases found in all the specimens were calcium silicate hydrate, quartz, and magnesioferrite. The quartz and magnesioferrite phases of the fly ash and RHA are usually observed in synthesized geopolymers [44–47], indicating that both the unreacted fly ash and RHA are present in the final geopolymeric composites. In this study, the amorphous aluminosilicate nature of the specimens was indicated by the diffuse halo peaks around 10–38° (2θ). Similar findings for metakaolin-based geopolymer pastes were reported by Kouamo et al. [45]. Clearly, a decrease in the sharpness of the hump peaks at around 10–20° (2θ) was observed when either hydrated borax or anhydrous borax was added (Fig. 4). The results were in agreement with those by Bagheri et al. [14]. However, there was no difference in the XRD patterns between the specimens containing 20% hydrated borax and those with 20% anhydrous borax.

Fig. 5 shows the effect of incorporating RHA on the phase composition of the geopolymer. It was found that the amorphous phase was affected by the addition of RHA. Obviously, an increase in the intensity of the peaks at around 10–20° (2θ) was obtained when the RHA was incorporated. This indicated that the amount of the amorphous phase in the specimen with RHA was higher than that in the specimen without
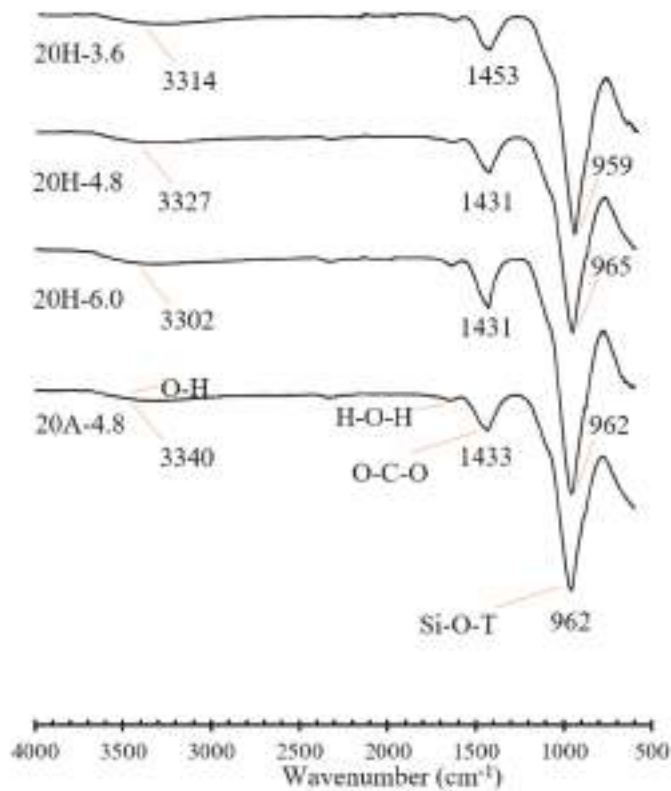
Fig. 7. figFTIR results for geopolymers made with RHA.

RHA. The increased amorphous phase could strengthen the structure because of the presence of high contents of geopolymer products [14]. A minor change in the XRD patterns was the decrease in the intensity of the peak at 32.05° (2θ), which was assigned to the C–S–H phase. Therefore, it was reasonable to assume that the inclusion of RHA resulted in favorable conditions for the formation of amorphous products rather than the C–S–H gel. However, the XRD patterns of the pastes made with RHA did not show an obvious change when the amount of RHA was increased from 3.6 to 6.0%. The results presented in Fig. 5 also show that the influence of RHA on the phase composition of the specimen made from anhydrous borax (20A-4.8) was the same as that on the specimen containing hydrated borax (20H-4.8).

3.2. FTIR analysis

The FTIR results of the geopolymer pastes are shown in Fig. 6 and Fig. 7. These results show that the geopolymer pastes consisted of broad bands located at 3700–3200 cm^{-1}, which were assigned to the stretching vibration of water molecules [48,49]. The broad band at 1700–1600 cm^{-1} represented the bending vibration (H–O–H) resulting from the adsorbed water molecules [50,51]. These vibrational modes indicate the formation of an aluminosilicate network in the geopolymer structure [50,52]. The occurrence of the CO_3^{2-} band, which occurs at approximately 1460 cm^{-1}, was detected in all the specimens as a result of the carbonation process between unreacted Na$_2$O and CO$_2$ in the environment [53,54]. Previous studies on geopolymers made with borax showed that the main B–O stretching bonds were observed in the wavenumber range of 1380–1310 cm^{-1} [6,55]. However, in the present study, the B–O bond was not detected in the FTIR analysis, probably because the borax content was insufficient. Bagheri et al. [14] suggested
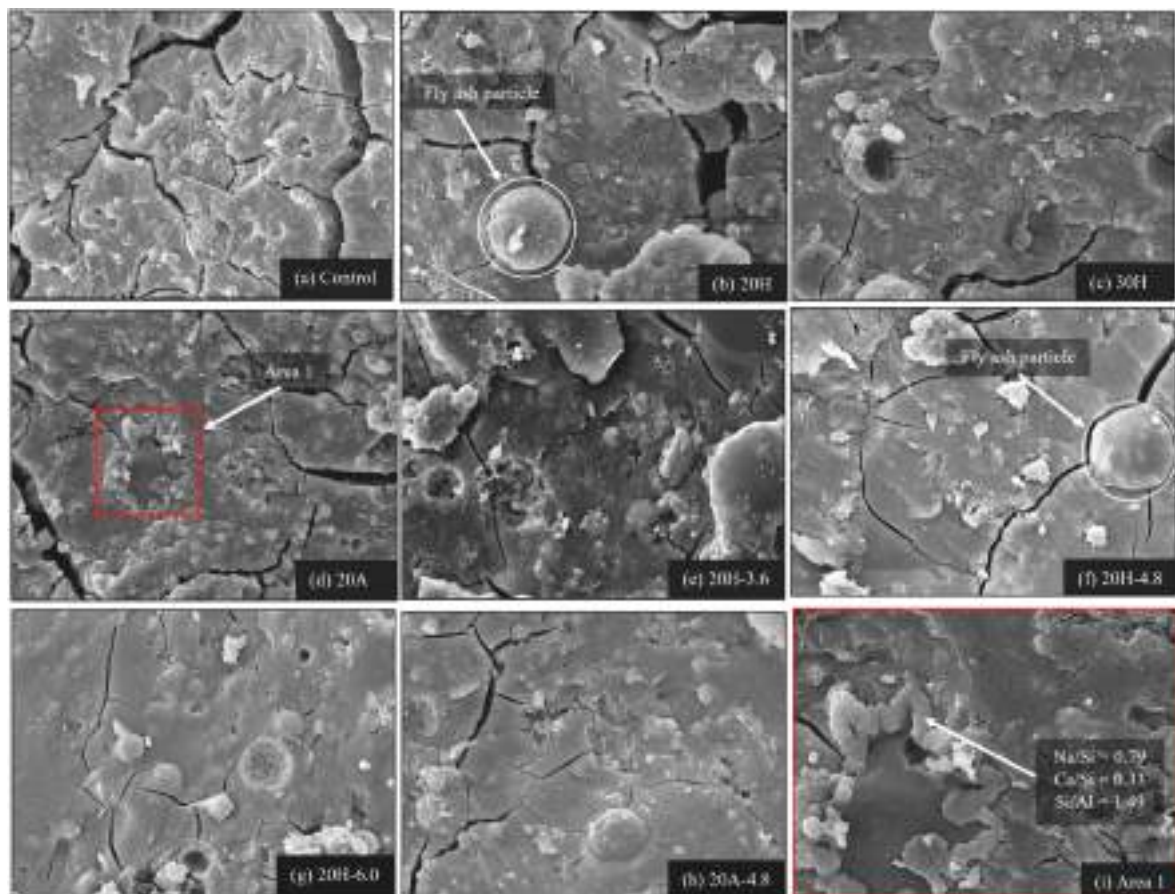
Fig. 8. SEM micrographs of geopolymer specimens.

Table 3
Atomic percentages and ratios of hardened geopolymer pastes based on EDS analyses.

Sample	Atom percentages and ratios						
	Na, at%	Ca, at%	Si, at%	Al, at%	Na/Si	Ca/Si	Si/Al
Control	11.27	7.68	9.53	4.40	1.18	0.81	2.17
10H	11.44	8.55	10.20	4.83	1.12	0.84	2.11
20H	12.99	6.76	9.83	4.99	1.32	0.70	1.97
30H	12.66	6.57	10.08	5.18	1.26	0.65	1.95
20H-3.6	8.67	7.95	8.94	3.41	0.97	0.89	2.62
20H-4.8	7.95	10.62	11.40	4.15	0.70	0.93	2.75
20H-6.0	8.86	8.25	11.61	4.25	0.76	0.71	2.73
20A	10.92	5.17	10.61	5.48	1.03	0.50	1.94
20A-4.8	9.25	8.47	11.16	3.86	0.83	0.76	2.89

that the formation of B–O bonds in geopolymer matrices is essential to prevent an unexpected strength behavior caused by the disruption of the balance in an alkaline activator.

An obvious change in the FTIR spectra of the geopolymer specimens made with borax occurred in the stretching bond at the wave number range of 1200–950 cm^{-1}. The Si–O-T vibration, in which "T" could be silicon (Si) and aluminum (Al) [6,55,56], is frequently used in the assessment of the degree of geopolymerization. The exact position of the broad band assigned to the Si–O-T stretching bond varies with the silicon (Si)/aluminum (Al) ratio of the specimen [57,58]. Generally, this band moves downward as a result of an increase in the Al content incorporated into the gel phase [52,58]. As shown in this study, the sharpness increased with increasing borax content (Fig. 6), indicating that a relatively high early release of Al species in the system was obtained with the inclusion of borax. A similar finding was reported for a low-calcium fly ash geopolymer paste [16]. De Silva et al. [59] suggested that an increase in the content of the tetrahedrally positioned Al atom (low Si/Al) led to geopolymers with low strengths.

In specimens containing hydrated borax and RHA (Fig. 7), the position of the band assigned to the Si–O-T bond shifted toward higher wavenumbers compared to the 20H mixture (see Fig. 6). These findings were supported by those of previous researchers working on geopolymers containing silica fume [57]. It should be noted that among the three mixtures, the 20H-4.8 specimen exhibited the highest wavenumber for the Si–O-T band in the chain structure of the binding phase. In addition, upon activation of the 20A-4.8 mixture, the band shifted to a higher wavenumber compared with the 20A mixture. These results indicated that the formation of a gel phase with a higher degree of crosslinking was obtained when the RHA was used. This could have been due to the greater silicate species in the aluminosilicate condensation process [60], which increased the amorphous content of the products.

3.3. SEM observations

SEM images of selected geopolymer paste specimens are shown in Fig. 8. The geopolymer specimens showed voids and unreacted fly ash particles, which were embedded in the continuous mass of the cementitious matrix. In addition, microcracks were clearly observed on the surfaces of all the specimens. The cracks formed in the control mixture (see Fig. 8(a)) may have been the result of moisture removal during the curing process rather than being load-induced cracks. Rapid drying during heat curing generated cracks in the form of "alligator skin". However, the results showed that significantly fewer cracks were observed in the specimens containing either hydrated borax (Fig. 8(b) and (c)) or anhydrous borax (Fig. 8(d)) compared to the control mixture, probably because the geopolymers with higher borax contents had relatively lower amounts of the liquid-containing compound (sodium silicate) and possibly because of the high moisture retention of borax [61]. Thus, it is no exaggeration to say that the inclusion of borax reduced thermal cracking. Moreover, the results showed that using anhydrous borax caused crystalline products with a low Si/Al ratio to form (see Fig. 8(d) and (i)), which will be discussed later.

The results shown in Fig. 8(e) and (h) show that the inclusion of RHA led to some differences in the matrix microstructures. The geopolymers with RHA showed a microstructure comprising a uniformly distributed dense gel phase and unreacted particles. Compared with the 20A mixture, the binding gel phase formed in the 20A-4.8 mixture (Fig. 8(h)) showed a more homogeneous morphology. This indicated that the microstructures of geopolymers made from borax can be improved by including RHA. However, the microstructural features of specimens with RHA contents >3.6% did not change significantly when the RHA content was increased. The results also showed that the cracks induced by external loading were blocked by the unreacted fly ash particles, as clearly seen in Fig. 8(b) and (f). Cracking around the spheres can be observed in several fly ash-based geopolymer systems [6,14,62], which results in more energy being dissipated during loading.

3.4. X-ray microanalysis (EDS)

Table 3 lists the elemental compositions at selected areas of the geopolymer gel phases (free from the unreacted fly ash particles) as derived from the EDS microanalysis. The values presented in the table are the averages of 2–3 analyses. In addition to sodium (Na), silicon (Si), and aluminum (Al), calcium (Ca) was also observed in all the geopolymer specimens. This indicated that the coexistence of an amorphous alkali aluminosilicate gel with a C–S–H phase was possible, as suggested by other studies [52,63,64]. In addition, the presence of a C–S–H type gel was supported by the XRD patterns shown in Figs. 4 and 5. In the
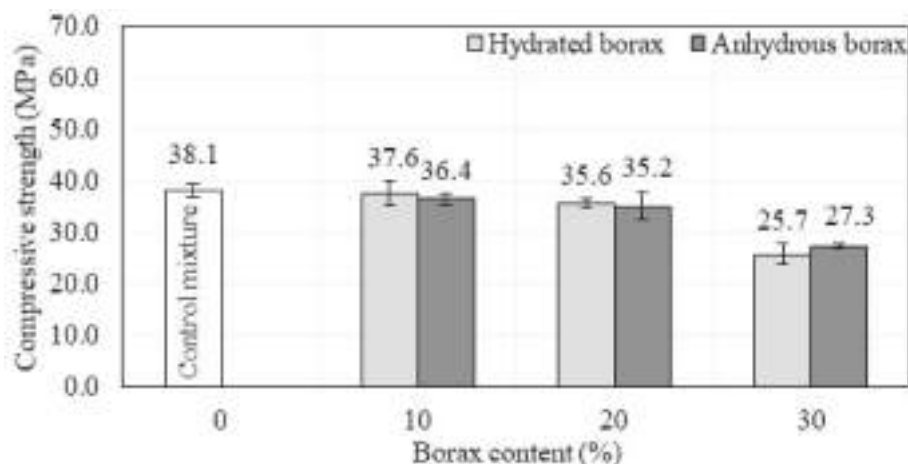
Fig. 9. Effects of borax content on compressive strengths of geopolymer mortars.
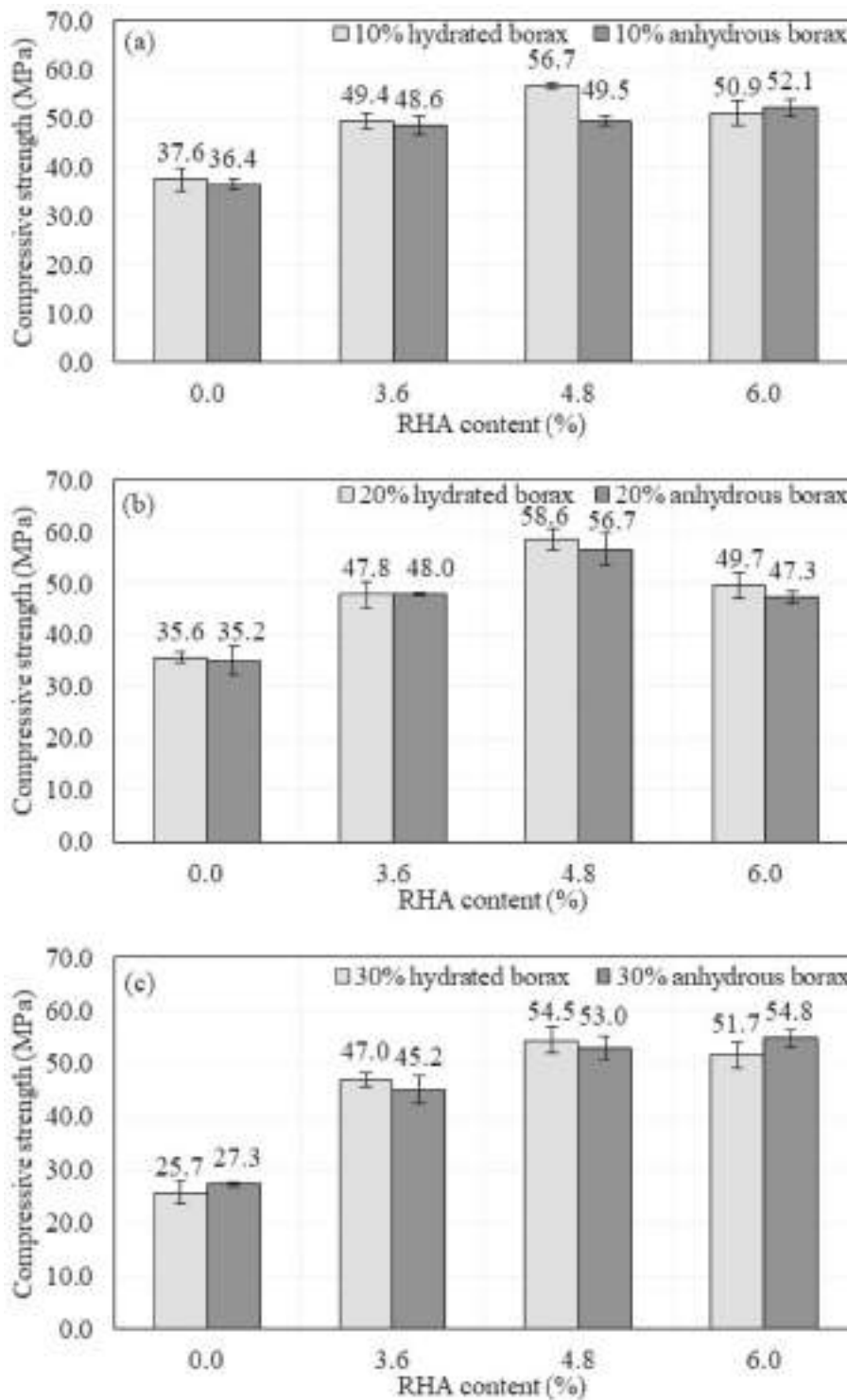
Fig. 10. Effects of RHA on compressive strengths of geopolymer mortars containing (a) 10% borax, (b) 20% borax, and (c) 30% borax.

present study, amorphous aluminosilicate was the main reaction product identified in the geopolymers; however, there was a significant difference in the elemental compositions of these aluminosilicate phases in specimens formed with borax and RHA.

The Si/Al ratio for the gel phase formed in the control mixture was 2.17 on average, while the Na/Si and Ca/Si ratios were 1.18 and 0.81, respectively. However, including either hydrated borax or anhydrous borax in the mix decreased the Si/Al ratio, partly because of the lower content of sodium silicate and partly inconsequence of the increase in Al

content dissolved from fly ash, which was consistent with the previously discussed FTIR results (Fig. 6). The Si/Al atomic ratios for the 10H, 20H, and 30H specimens were in the range of 1.95–2.11. Moreover, it was found that the Si/Al atomic ratio of the gel phases for the 20A specimen was 1.94, which was close to 2. According to Davidovits [65], who classified the type of geopolymer structure based on the Si/Al ratio, it is possible that the main geopolymeric gel observed in the system made from borax was (Na)-poly(sialate-siloxo).

Another interesting phenomenon is that the incorporation of
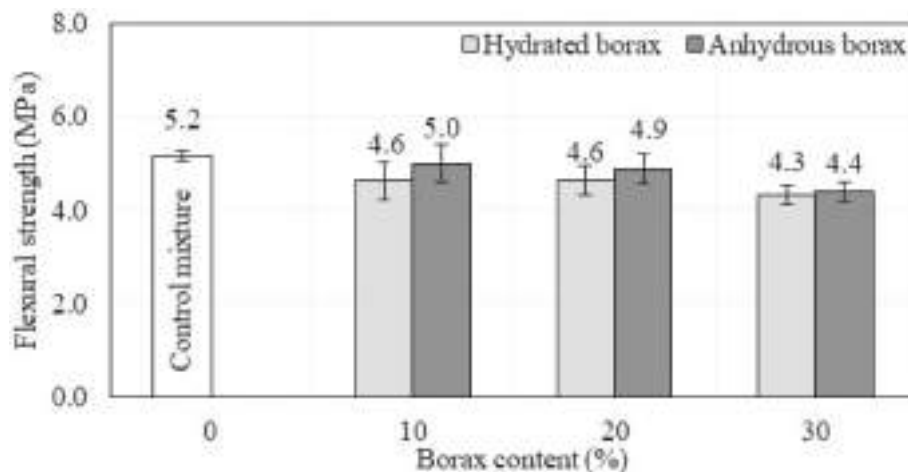
Fig. 11. Effects of borax content on flexural strengths of geopolymer mortars.

anhydrous borax resulted in the formation of crystalline hydrate phases with a low Si/Al ratio (see Fig. 8(i)), which had detrimental effects on the strengths of the geopolymers. As shown in this study (Table 3), the use of borax reduced the availability of the Ca^{2+} dissolved from the fly ash. The role of Ca^{2+} is important in hindering the formation of crystalline sodium aluminosilicate (zeolitic) phases, which are detrimental to the strength [27]. However, the peaks of the sodium-based zeolitic phase could not be detected in the XRD analysis because the peaks were weak and overlapped with the position of quartz [26,66].

The Si/Al atomic ratios of the gel phases for the 20H-3.6, 20H-4.8, and 20H-6.0 specimens were 2.62, 2.75, and 2.73, respectively, which were higher than that of the 20H specimen (1.97). It could be deduced from the results that the additional Si dissolved from the RHA contributed to the formation of a binding gel phase, producing a 3D rigid polymeric structure [59]. This was supported by the shifting of the Si–O-T band, as identified from the FTIR results, which showed that the position of this band shifted to a higher wavenumber when the RHA was incorporated. A similar trend was found in the case of specimens containing anhydrous borax. A higher Si/Al ratio could be observed in the specimen with RHA when a comparison was made between the Si/Al ratios of the 20A-4.8 and 20A mixtures.

Another important change in the elemental compositions of the geopolymers made with RHA was the consumption of Ca^{2+} ions in the geopolymerization process. The Ca/Si ratio of the gel phase in the specimens was found to increase with the use of RHA. It is possible that more Ca^{2+} ions dissolved from the fly ash were consumed during the reaction process when RHA was added [27]. The increased content of Ca incorporated into the N-A-S-H type gel derived from the activation of the fly ash in the presence of RHA was consistent with the XRD spectra, which suggested the reduction of the C–S–H type gel within the binding phase, along with the formation of a geopolymer product with a higher amorphous content.

3.5. Compressive strength

Fig. 9 and Fig. 10 show the influence of the borax and RHA contents on the compressive strengths of the geopolymer mortars, respectively. Including either hydrated borax or anhydrous borax in the mixture tended to reduce the compressive strength, especially with a 30% borax replacement. Compared with the control mixture, the specimens with 30% hydrated borax and 30% anhydrous borax showed compressive strength decreases of 33% and 28%, respectively. This was in agreement with the trends previously reported for low-calcium fly ash-based geopolymer systems [14,15]. The reduction in the compressive strength of a geopolymer prepared with borax may be understood as a decrease in the Si/Al ratio of the gel phase formed in the system, which led to an

increase in the crystalline nature of the geopolymer, as evidenced by the XRD results. However, the presence of borax appeared to hinder the formation of cracks due to water evaporation during heat curing. This may explain why the compressive strength of the mortar containing ≤20% borax was close to that of the control mortar.

The compressive strength was also measured for geopolymer mortar specimens containing various percentages of RHA (Fig. 10). The results showed that there was an increase in the compressive strength with an increase in the RHA content from 3.6% to 6.0% in the mixtures prepared with borax. The incorporation of RHA increased the Si/Al ratio and resulted in the formation of more cross-linked binding gels. The increase in compressive strength resulting from increasing the Si/Al ratio has been linked to an improvement in the microstructural homogeneity. The SEM images provided evidence that the change in the homogeneity of the geopolymer was associated with a change in the RHA content (see Fig. 8). The microstructural features of the specimens were observed to be largely homogeneous for RHA contents ≥ 3.6% (Si/Al ratios > 2.17), resulting in geopolymers with higher strength.

3.6. Flexural strength

The flexural strength results for the geopolymer mortars are shown in Figs. 11 and 12. Similar to the compressive strength discussed earlier, the use of borax to replace sodium silicate tended to reduce the flexural strength, mainly because a binding gel with a lower Si/Al ratio was produced and possibly as a result of the absence of B–O bonds, which would encourage the development of strength [6,55]. When the borax content was increased beyond 20%, a significant reduction in flexural strength was observed. The flexural strength values of mortar mixtures 30H and 30A decreased by 16% and 15%, respectively, relative to the control mortar. The results also indicated that the flexural strengths of mortars with hydrated borax were close to those of mortars with anhydrous borax (Fig. 11). In addition, it should be noted that the negative effects of borax inclusion were less pronounced for the flexural strength than for the compressive strength of the mortar.

In relation to the use of RHA in the geopolymer mortars containing borax (Fig. 12), the trends in the flexural strength of the mortars were similar to those for the compressive strength. Adding RHA increased the strength, not only because of the increase in the Si/Al ratio, but also because of the higher calcium content, which became incorporated in the N-A-S-H gel. The optimum RHA content was found to be 4.8% (by weight of fly ash). For example, the addition of 3.6%, 4.8%, and 6.0% RHA increased the flexural strength of the 30H mixture by approximately 22%, 39%, and 31%, respectively. In addition, geopolymer mortars with an RHA content of 4.8% showed an approximately 17–22% higher flexural strength than the control mortar. However, the trend of
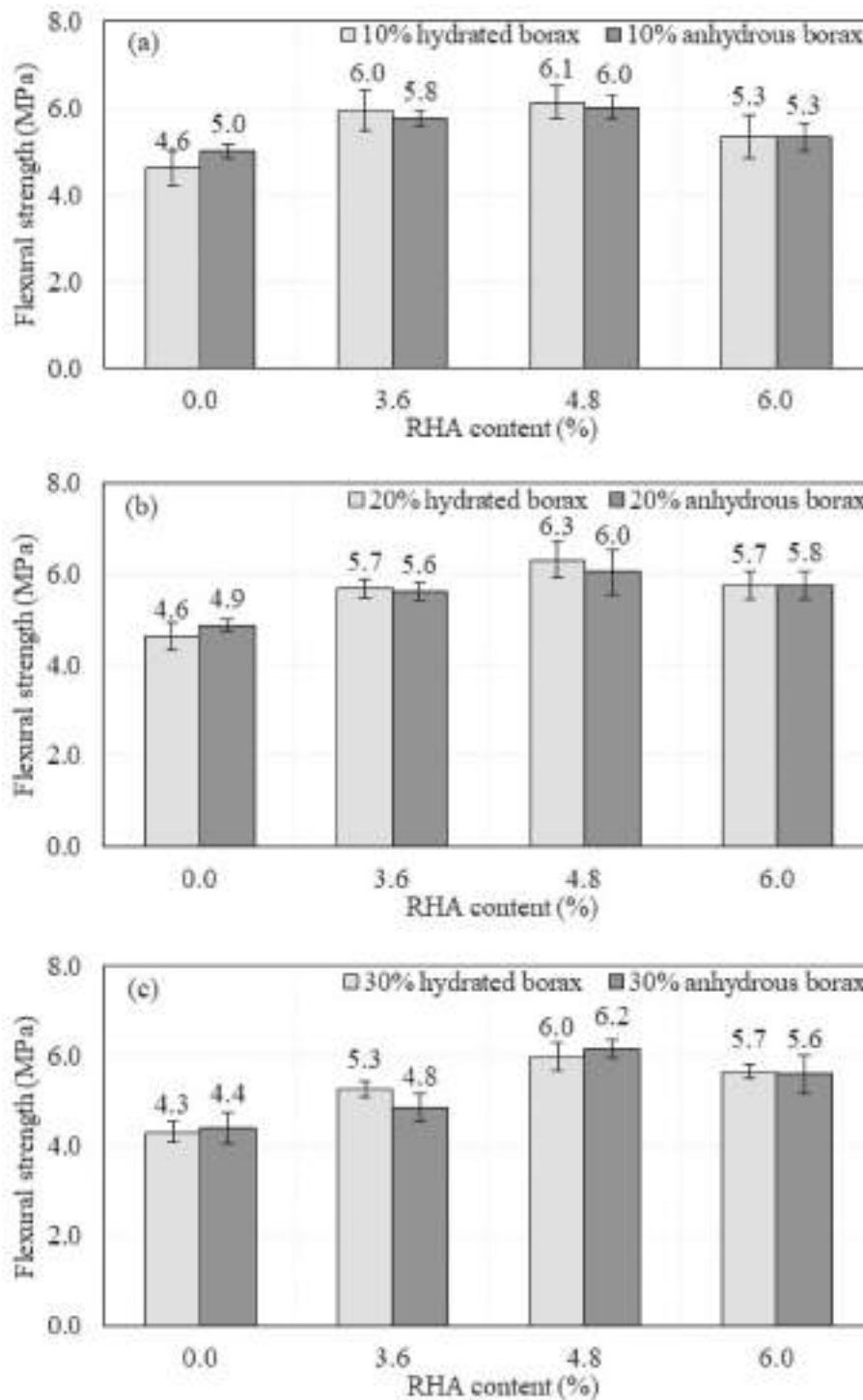
Fig. 12. Effects of RHA on flexural strengths of geopolymer mortars containing (a) 10% borax, (b) 20% borax, and (c) 30% borax.

decreasing the strengths with the RHA inclusion was observed when the content of RHA increased beyond 4.8%, because the presence of excessive soluble silicate may impede geopolymer structure formation [67].

4. Conclusion

This study developed geopolymers with lower amounts of sodium silicate, while maintaining the performance requirements. Borax, instead of sodium silicate, was used as an activator for high-calcium fly

ash geopolymers. RHA was added to compensate for the strength-reducing effect of the borax in the geopolymers. Based on the experimental results presented here, the following conclusions can be drawn.

(1) The main reaction products of the geopolymers made with borax were an N-A-S-H type gel. The results showed that the Si/Al ratio of the gel phase decreased as the borax content in the mixture increased. In addition, there was a decrease in the availability of calcium due to the dissolution of fly ash when the borax content was increased from 0% to 30%. However, the presence of borax

appeared to hinder the formation of cracks due to moisture removal during the heat curing process, thus reducing its detrimental effect on the strengths.

(2) The incorporation of RHA into geopolymers made with borax resulted in the formation of a Ca-modified N-A-S-H gel with a high Si/Al ratio. The increase in the Si/Al ratio of the binding gel due to the presence of RHA caused an improvement in the microstructural homogeneity. When RHA was present in the system, the calcium dissolved from the high-calcium fly ash first tended to form a Ca-modified N-A-S-H gel rather than the C–S–H phase. The modification of the elemental composition of the binding gel phase was believed to be a reason for the strength development.

(3) Incorporating either hydrated borax or anhydrous borax in the geopolymer mixture decreased both the compressive and flexural strengths, especially with the 30% borax replacement. However, the detrimental effect appeared to be more pronounced for the compressive strength. The results also showed that the strengths of the geopolymer mortars made from hydrated borax were comparable to those of the mortars containing anhydrous borax.

(4) RHA could be used to improve the strengths of the geopolymer mortars containing either hydrated borax or anhydrous borax. The optimum amount of RHA was approximately 4.8% by weight of fly ash. The use of 4.8% RHA improved the compressive and flexural strengths of the geopolymer mortars made with borax by 30–54% and 17–22% compared to those of the control mortar, respectively.

CRediT authorship contribution statement

Peem Nuaklong: Conceptualization, Methodology, Investigation, Writing – original draft, Writing – review & editing, Visualization. **Kit Janprasit:** Investigation. **Pitcha Jongvivatsakul:** Conceptualization, Methodology, Investigation, Resources, Writing – original draft, Writing – review & editing, Supervision, Project administration, Funding acquisition.

Declaration of competing interest

The authors declare that they have no known competing financial interests or personal relationships that could have appeared to influence the work reported in this paper.

Acknowledgement

References

[1] L.K. Turner, F.G. Collins, Carbon dioxide equivalent (CO_2-e) emissions: a comparison between geopolymer and OPC cement concrete, Construct. Build. Mater. 43 (2013) 125–130, https://doi.org/10.1016/j.conbuildmat.2013.01.023.

[2] B.C. McLellan, R.P. Williams, J. Lay, A. Van Riessen, G.D. Corder, Costs and carbon emissions for geopolymer pastes in comparison to ordinary portland cement, J. Clean. Prod. 19 (9–10) (2011) 1080–1090, https://doi.org/10.1016/j.jclepro.2011.02.010.

[3] G. Habert, J.D.E. De Lacaillerie, N. Roussel, An environmental evaluation of geopolymer based concrete production: reviewing current research trends, J. Clean. Prod. 19 (11) (2011) 1229–1238, https://doi.org/10.1016/j.jclepro.2011.03.012.

[4] F.N. Okoye, S. Prakash, N.B. Singh, Durability of fly ash based geopolymer concrete in the presence of silica fume, J. Clean. Prod. 149 (2017) 1062–1067, https://doi.org/10.1016/j.jclepro.2017.02.176.

[5] K. Neupane, Fly ash and GGBFS based powder-activated geopolymer binders: a viable sustainable alternative of Portland cement in concrete industry, Mech. Mater. 103 (2016) 110–122, https://doi.org/10.1016/j.mechmat.2016.09.012.

[6] A. Nazari, A. Maghsoudpour, J.G. Sanjayan, Characteristics of boroaluminosilicate geopolymers, Construct. Build. Mater. 70 (2014) 262–268, https://doi.org/10.1016/j.conbuildmat.2014.07.087.

[7] J.L. Provis, C.Z. Yong, P. Duxson, J.S. van Deventer, Correlating mechanical and thermal properties of sodium silicate-fly ash geopolymers, Colloids Surf., A 336 (1–3) (2009) 57–63, https://doi.org/10.1016/j.colsurfa.2008.11.019.

[8] F. Puertas, M. Torres-Carrasco, Use of glass waste as an activator in the preparation of alkali-activated slag, Mechanical strength and paste characterisation, Cement Concr. Res. 57 (2014) 95–104, https://doi.org/10.1016/j.cemconres.2013.12.005.

[9] J. Shi, J. Tan, B. Liu, J. Chen, J. Dai, Z. He, Experimental study on full-volume slag alkali-activated mortars: Air-cooled blast furnace slag versus machine-made sand as fine aggregates, J. Hazard Mater. 403 (2021) 123983, https://doi.org/10.1016/j.jhazmat.2020.123983.

[10] J. Shi, B. Liu, Z. He, Y. Liu, J. Jiang, T. Xiong, J. Shi, A green ultra-lightweight chemically foamed concrete for building exterior: a feasibility study, J. Clean. Prod. 288 (2021) 125085, https://doi.org/10.1016/j.jclepro.2020.125085.

[11] F. Pacheco-Torgal, Z. Abdollahnejad, A.F. Camões, M. Jamshidi, Y. Ding, Durability of alkali-activated binders: a clear advantage over Portland cement or an unproven issue? Construct. Build. Mater. 30 (2012) 400–405, https://doi.org/10.1016/j.conbuildmat.2011.12.017.

[12] K.T. Tong, R. Vinai, M.N. Soutsos, Use of Vietnamese rice husk ash for the production of sodium silicate as the activator for alkali-activated binders, J. Clean. Prod. 201 (2018) 272–286, https://doi.org/10.1016/j.jclepro.2018.08.025.

[13] E. Kamseu, L.B. à Moungam, M. Cannio, N. Billong, D. Chaysuwan, U.C. Melo, C. Leonelli, Substitution of sodium silicate with rice husk ash-NaOH solution in metakaolin based geopolymer cement concerning reduction in global warming, J. Clean. Prod. 142 (2017) 3050–3060, https://doi.org/10.1016/j.jclepro.2016.10.164.

[14] A. Bagheri, A. Nazari, J.G. Sanjayan, P. Rajeev, Alkali activated materials vs geopolymers: role of boron as an eco-friendly replacement, Construct. Build. Mater. 146 (2017) 297–302, https://doi.org/10.1016/j.conbuildmat.2017.04.137.

[15] A. Bagheri, A. Nazari, J.G. Sanjayan, P. Rajeev, W. Duan, Fly ash-based boroaluminosilicate geopolymers: experimental and molecular simulations, Ceram. Int. 43 (5) (2017) 4119–4126, https://doi.org/10.1016/j.ceramint.2016.12.020.

[16] A. Bagheri, A. Nazari, A. Hajimohammadi, J.G. Sanjayan, P. Rajeev, M. Nikzad, . P. Mendis, Microstructural study of environmentally friendly boroaluminosilicate geopolymers, J. Clean. Prod. 189 (2018) 805–812, https://doi.org/10.1016/j.jclepro.2018.04.034.

[17] J. Prasara-A, S.H. Gheewala, Sustainable utilization of rice husk ash from power plants: a review, J. Clean. Prod. 167 (2017) 1020–1028, https://doi.org/10.1016/j.jclepro.2016.11.042.

[18] R. Pode, Potential applications of rice husk ash waste from rice husk biomass power plant, Renew. Sustain. Energy Rev. 53 (2016) 1468–1485, https://doi.org/10.1016/j.rser.2015.09.051.

[19] C. Sookkumnerd, N. Ito, K. Kito, bFeasibility of husk-fuelled steam engines as prime mover of grid-connected generators under the Thai very small renewable energy power producer (VSPP) program, J. Clean. Prod. 15 (3) (2007) 266–274, https://doi.org/10.1016/j.jclepro.2006.02.003.

[20] B. Sajjakulnukit, R. Yingyuad, V. Maneekhao, V. Pongnarintasut, S. C. Bhattacharya, P.A. Salam, Assessment of sustainable energy potential of non-plantation biomass resources in Thailand, Biomass Bioenergy 29 (3) (2005) 214–224, https://doi.org/10.1016/j.biombioe.2005.03.009.

[21] D.G. Nair, A. Fraaij, A.A. Klaassen, A.P. Kentgens, A structural investigation relating to the pozzolanic activity of rice husk ashes, Cement Concr. Res. 38 (6) (2008) 861–869, https://doi.org/10.1016/j.cemconres.2007.10.004.

[22] E. Aprianti, P. Shafigh, S. Bahri, J.N. Farahani, Supplementary cementitious materials origin from agricultural wastes–A review, Construct. Build. Mater. 74 (2015) 176–187, https://doi.org/10.1016/j.conbuildmat.2014.10.010.

[23] Z.H. He, L.Y. Li, S.G. Du, Creep analysis of concrete containing rice husk ash, Cement Concr. Compos. 80 (2017) 190–199, https://doi.org/10.1016/j.cemconcomp.2017.03.014.

[24] A. Kusbiantoro, M.F. Nuruddin, N. Shafiq, S.A. Qazi, The effect of microwave incinerated rice husk ash on the compressive and bond strength of fly ash based geopolymer concrete, Construct. Build. Mater. 36 (2012) 695–703, https://doi.org/10.1016/j.conbuildmat.2012.06.064.

[25] C.L. Hwang, T.P. Huynh, Effect of alkali-activator and rice husk ash content on strength development of fly ash and residual rice husk ash-based geopolymers, Construct. Build. Mater. 101 (2015) 1–9, https://doi.org/10.1016/j.conbuildmat.2015.10.025.

[26] P. Nuaklong, P. Jongvivatsakul, T. Pothisiri, V. Sata, P. Chindaprasirt, Influence of rice husk ash on mechanical properties and fire resistance of recycled aggregate high-calcium fly ash geopolymer concrete, J. Clean. Prod. 252 (2020), https://doi.org/10.1016/j.jclepro.2019.119797, 119797.

[27] P. Chindaprasirt, P. De Silva, K. Sagoe-Crentsil, S. Hanjitsuwan, Effect of SiO_2 and Al_2O_3 on the setting and hardening of high calcium fly ash-based geopolymer systems, J. Mater. Sci. 47 (12) (2012) 4876–4883, https://doi.org/10.1007/s10853-012-6353-y.

[28] P. Duxson, J.L. Provis, G.C. Lukey, S.W. Mallicoat, W.M. Kriven, J.S. Van Deventer, Understanding the relationship between geopolymer composition, microstructure and mechanical properties, Colloids Surf., A 269 (1–3) (2005) 47–58, https://doi.org/10.1016/j.colsurfa.2005.06.060.

[29] T.H.A. Al Saadi, A.I. Badanoiu, A.I. Nicoara, S. Stoleriu, G. Voicu, Synthesis and properties of alkali activated borosilicate inorganic polymers based on waste glass, Construct. Build. Mater. 136 (2017) 298–306, https://doi.org/10.1016/j.conbuildmat.2017.01.026.

[30] R.P. Williams, A. van Riessen, Development of alkali activated borosilicate inorganic polymers (AABSIP), J. Eur. Ceram. Soc. 31 (8) (2011) 1513–1516, https://doi.org/10.1016/j.jeurceramsoc.2011.02.021.

[31] ASTM C33/C33M-18, Standard Specification for Concrete Aggregates, ASTM International, West Conshohocken, United States, 2018.

[32] ASTM C136/C136M-19, Standard Test Method for Sieve Analysis of Fine and Coarse Aggregates, ASTM International, West Conshohocken, United States, 2019.

[33] ASTM C128-15, Standard Test Method for Relative Density (Specific Gravity) and Absorption of Fine Aggregate, ASTM International, West Conshohocken, United States, 2015.

[34] ASTM C29/C29M-17, Standard Test Method for Bulk Density ("Unit Weight") and Voids in Aggregate, ASTM International, West Conshohocken, United States, 2017.

[35] I. Waclawska, Thermal decomposition of borax, J. Therm. Anal. Calorim. 43 (1) (1995) 261–269, https://doi.org/10.1007/bf02635993.

[36] ASTM C109/C109M-16, Standard Test Method for Compressive Strength of Hydraulic Cement Mortars (Using 2-in. Or [50-mm] Cube Specimens), ASTM International, West Conshohocken, United States, 2016.

[37] P. Chindaprasirt, T. Chareerat, V. Sirivivatnanon, Workability and strength of coarse high calcium fly ash geopolymer, Cement Concr. Compos. 29 (3) (2007) 224–229, https://doi.org/10.1016/j.cemconcomp.2006.11.002.

[38] P. Nuaklong, V. Sata, P. Chindaprasirt, Influence of recycled aggregate on fly ash geopolymer concrete properties, J. Clean. Prod. 112 (2016) 2300–2307, https://doi.org/10.1016/j.jclepro.2015.10.109.

[39] P. Nuaklong, V. Sata, P. Chindaprasirt, Properties of metakaolin-high calcium fly ash geopolymer concrete containing recycled aggregate from crushed concrete specimens, Construct. Build. Mater. 161 (2018) 365–373, https://doi.org/10.1016/j.conbuildmat.2017.11.152.

[40] P. Nuaklong, V. Sata, A. Wongsa, K. Srinavin, P. Chindaprasirt, Recycled aggregate high calcium fly ash geopolymer concrete with inclusion of OPC and nano-SiO2, Construct. Build. Mater. 174 (2018) 244–252, https://doi.org/10.1016/j.conbuildmat.2018.04.123.

[41] P. Nuaklong, A. Wongsa, V. Sata, K. Boonserm, J. Sanjayan, P. Chindaprasirt, Properties of high-calcium and low-calcium fly ash combination geopolymer mortar containing recycled aggregate, Heliyon 5 (9) (2019), e02513, https://doi.org/10.1016/j.heliyon.2019.e02513.

[42] P. Nuaklong, A. Wongsa, K. Boonserm, C. Ngohpok, P. Jongvivatsakul, V. Sata, . P. Chindaprasirt, Enhancement of mechanical properties of fly ash geopolymer containing fine recycled concrete aggregate with micro carbon fiber, J. Build. Eng. 41 (2021) 102403, https://doi.org/10.1016/j.jobe.2021.102403.

[43] ASTM C348-19, Standard Test Method for Flexural Strength of Hydraulic-Cement Mortars, ASTM International, West Conshohocken, United States, 2019.

[44] H. Xu, W. Gong, L. Syltebo, K. Izzo, W. Lutze, L.L. Pegg, Effect of blast furnace slag grades on fly ash based geopolymer waste forms, Fuel 133 (2014) 332–340, https://doi.org/10.1016/j.fuel.2014.05.018.

[45] H.T. Kouamo, A. Elimbi, J.A. Mbey, C.N. Sabouang, D. Njopwouo, The effect of adding alumina-oxide to metakaolin and volcanic ash on geopolymer products: a comparative study, Construct. Build. Mater. 35 (2012) 960–969, https://doi.org/10.1016/j.conbuildmat.2012.04.023.

[46] Z. Zidi, M. Ltifi, I. Zafar, Synthesis and attributes of nano-SiO2 local metakaolin based-geopolymer, J. Build. Eng. 33 (2021) 101586, https://doi.org/10.1016/j.jobe.2020.101586.

[47] S.K. Das, S.M. Mustakim, A. Adesina, J. Mishra, T.S. Alomayri, H.S. Assaedi, C. R. Kaze, Fresh, strength and microstructure properties of geopolymer concrete incorporating lime and silica fume as replacement of fly ash, J. Build. Eng. 32 (2020) 101780, https://doi.org/10.1016/j.jobe.2020.101780.

[48] M. Eiamwijit, K. Pachana, S. Kaewpirom, U. Rattanasak, P. Chindaprasirt, Comparative study on morphology of ground sub-bituminus FBC fly ash geopolymeric material, Adv. Powder Technol. 26 (4) (2015) 1053–1057, https://doi.org/10.1016/j.apt.2015.04.013.

[49] M. Vafaei, A. Allahverdi, High strength geopolymer binder based on waste-glass powder, Adv. Powder Technol. 28 (1) (2017) 215–222, https://doi.org/10.1016/j.apt.2016.09.034.

[50] T. Bakharev, Geopolymeric materials prepared using Class F fly ash and elevated temperature curing, Cement Concr. Res. 35 (6) (2005) 1224–1232, https://doi.org/10.1016/j.cemconres.2004.06.031.

[51] K. Pimraksa, P. Chindaprasirt, A. Rungchet, K. Sagoe-Crentsil, T. Sato, Lightweight geopolymer made of highly porous siliceous materials with various Na2O/Al2O3 and SiO2/Al2O3 ratios, Mater. Sci. Eng. A. 528 (21) (2011) 6616–6623, https://doi.org/10.1016/j.msea.2011.04.044.

[52] K. Somna, C. Jaturapitakkul, P. Kajitvichyanukul, P. Chindaprasirt, NaOH-activated ground fly ash geopolymer cured at ambient temperature, Fuel 90 (6) (2011) 2118–2124, https://doi.org/10.1016/j.fuel.2011.01.018.

[53] K. Boonserm, V. Sata, K. Pimraksa, P. Chindaprasirt, Improved geopolymerization of bottom ash by incorporating fly ash and using waste gypsum as additive, Cement Concr. Compos. 34 (7) (2012) 819–824, https://doi.org/10.1016/j.cemconcomp.2012.04.001.

[54] P. Chindaprasirt, U. Rattanasak, C. Jaturapitakkul, Utilization of fly ash blends from pulverized coal and fluidized bed combustions in geopolymeric materials, Cement Concr. Compos. 33 (1) (2011) 55–60, https://doi.org/10.1016/j.cemconcomp.2010.09.017.

[55] A. Khezrloo, E. Aghaie, M. Tayebi, Split tensile strength of slag-based boroaluminosilicate geopolymer, J. Australas. Ceram. Soc. 54 (1) (2018) 65–70, https://doi.org/10.1007/s41779-017-0127-6.

[56] I. Garcia-Lodeiro, A. Palomo, A. Fernández-Jiménez, D.E. Macphee, Compatibility studies between NASH and CASH gels, Study in the ternary diagram Na2O–CaO–Al2O3–SiO2–H2O, Cement Concr. Res. 41 (9) (2011) 923–931, https://doi.org/10.1016/j.cemconres.2011.05.006.

[57] S. Yaseri, G. Hajiaghaei, F. Mohammadi, M. Mahdikhani, R. Farokhzad, The role of synthesis parameters on the workability, setting and strength properties of binary binder based geopolymer paste, Construct. Build. Mater. 157 (2017) 534–545, https://doi.org/10.1016/j.conbuildmat.2017.09.102.

[58] A. Fernández-Jiménez, A. Palomo, Mid-infrared spectroscopic studies of alkali-activated fly ash structure, Microporous Mesoporous Mater. 86 (1–3) (2005) 207–214, https://doi.org/10.1016/j.micromeso.2005.05.057.

[59] P. De Silva, K. Sagoe-Crenstil, V. Sirivivatnanon, Kinetics of geopolymerization: role of Al2O3 and SiO2, Cement Concr. Res. 37 (4) (2007) 512–518, https://doi.org/10.1016/j.cemconres.2007.01.003.

[60] I. Ismail, S.A. Bernal, J.L. Provis, R. San Nicolas, S. Hamdan, J.S. van Deventer, Modification of phase evolution in alkali-activated blast furnace slag by the incorporation of fly ash, Cement Concr. Compos. 45 (2014) 125–135, https://doi.org/10.1016/j.cemconcomp.2013.09.006.

[61] J. Wang, L. Han, Z. Liu, D. Wang, Setting controlling of lithium slag-based geopolymer by activator and sodium tetraborate as a retarder and its effects on mortar properties, Cem, Concr. Compos. (2020) 103598, https://doi.org/10.1016/j.cemconcomp.2020.103598.

[62] C. Tennakoon, A. Nazari, J.G. Sanjayan, K. Sagoe-Crentsil, Distribution of oxides in fly ash controls strength evolution of geopolymers, Construct. Build. Mater. 71 (2014) 72–82, https://doi.org/10.1016/j.conbuildmat.2014.08.016.

[63] X. Guo, H. Shi, W.A. Dick, Compressive strength and microstructural characteristics of class C fly ash geopolymer, Cement Concr. Compos. 32 (2) (2010) 142–147, https://doi.org/10.1016/j.cemconcomp.2009.11.003.

[64] J.V. Temuujin, A. Van Riessen, R. Williams, Influence of calcium compounds on the mechanical properties of fly ash geopolymer pastes, J. Hazard Mater. 167 (1–3) (2009) 82–88, https://doi.org/10.1016/j.jhazmat.2008.12.121.

[65] J. Davidovits, Geopolymer, Chemistry and Applications, third ed., Institut Geopolymer, Saint Quentin, 2008.

[66] S.A. Bernal, J.L. Provis, V. Rose, R.M. De Gutierrez, Evolution of binder structure in sodium silicate-activated slag-metakaolin blends, Cement Concr. Compos. 33 (1) (2011) 46–54, https://doi.org/10.1016/j.cemconcomp.2010.09.004.

[67] Q. Wan, F. Rao, S. Song, R.E. García, R.M. Estrella, C.L. Patino, Y. Zhang, Geopolymerization reaction, microstructure and simulation of metakaolin-based geopolymers at extended Si/Al ratios, Cem, Concr. Compos. 79 (2017) 45–52, https://doi.org/10.1016/j.cemconcomp.2017.01.014.

WORK EXPERIENCE

HOLLOW CORE SLAB DESIGN

Over 60,000 square meters of VCON Hollow Core Slabs were installed at IKEA Bangyai, the largest IKEA store in South East Asia, this project took 3 months to complete.

HOLLOW CORE SLAB DESIGN

Project:

Type of Slab (cm.)		Clear Span (m.)	Live Load (kg/m^2)	S Dead Load (kg/m^2)	PC. Strand (Amount/mm.)		Topping (em.)
VC	40	12	900	200	10	12.7	7.5

(1.2 m., width)
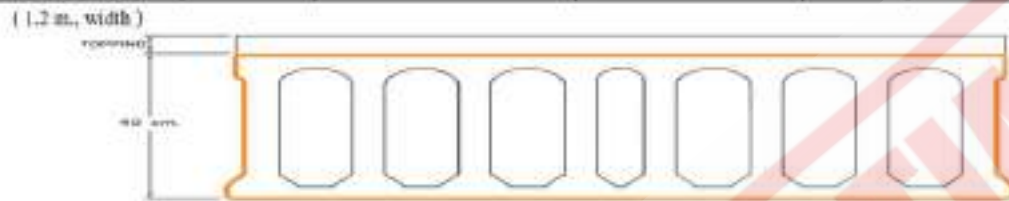
[1] DESIGN CRITERIA

Clear Span	=	12	m.	K=L^2/8	18.0000
Live Load	=	900	kg/m^2		
SuperImposed Dead Load	=	200	kg/m^2		

PC. STRAND INFO

PC. strand diameter	=	12.7	mm.	No. of strand	=	10	A$_{ps}$ (cm^2) = 9.871
Area per strand	=	0.987	cm^2	f$_{ps}$	=	18,960	kg/cm^2

MATERIAL PROPERTIES

	Plain	Topping	
Density of concrete =	2,400	2,400	kg/m^3
Initial Compressive Str. f'ci =	280	-	kg/cm^2
Initial Modulus of Elasticity, Eci =	265,659	-	kg/cm^2
Compressive Str. f'c =	400	240	kg/cm^2
Modulus of Elasticity, Ec =	317,523	245,952	kg/cm^2
Modulus ratio, n =	0.7746		

SECTION PROPERTIES

	Plain		Composit			Plain		Composit	
A	2,318	cm^2			w	463.70	kg/m^2	676.67	kg/m^2
I	437,581	cm^4	800,235.2	cm^4	e	16.30	cm.	22.81	cm.
Y$_b$	20.00	cm.	26.51	cm.	d	36.30	cm.	43.80	cm.
Y$_t$	20.00	cm.	20.99	cm.	b	116.80	cm.	120.00	cm.
Z$_b$	21,876	cm^3	30,181.00	cm^3	b$_w$	40.00	cm.	40.00	cm.
Z$_t$	21,882	cm^3	40,016.55	cm^3				3.70	cm.

HOLLOW CORE SLAB DESIGN

[2] DESIGN LOAD AND MOMENT

SERVICE LOAD (kg/m)			SERVICE MOMENT (kg-m)		
Slab weight, Wdl = 1.2x 464	=	556.44	$M_{dl} = W_{dl} \times K$ =		10,015.84 kg-m
Topping weight, Wtdl = 1.2x 213	=	255.56	$M_{tdl} = W_{tdl} \times K$ =		4,600.15 kg-m
SDL, Wsdl = 1.2x 200	=	240.00	$M_{sdl} = W_{sdl} \times K$ =		4,320.00 kg-m
Live Load, Wll = 1.2x 900	=	1,080.00	$M_{ll} = W_{ll} \times K$ =		19,440.00 kg-m
Total Dead Load, WTdl = 1.2x 877	=	1,052.00	$M_{Tdl} = W_{Tdl} \times K$ =		18,935.99 kg-m

[3] ULTIMATE LOAD ANALYSIS

LOAD COMBINATION

Load factor DL =	1.4	LL =	1.7		
W_u =	3,308.80 kg/m		$M_u = W_u \times K$ =		59,558.39 kg-m

PRESTRESSING REINFORCEMENT

PC.strand diameter	=	12.7	mm.	Amount of PC.std.	=	10	
Area of Prestressing steel, A_{ps}	=	9.8710	cm^2	Jacking force	=	70	%
Ultimate Prestressing stress, f_{pu}	=	18,960	kg/cm^2				
Initial Losses of Prestressed, K_1	=	10	%				
Final Losses of Prestressed, K_2	=	22	%				

				BONDED	DEBONDED
PRESTRESSING FORCE					2 strands
Initial Prestressing Force	P_i = Jacking force $\times f_{pu} \times A_{ps}$		=	131,007.91 kg	104,806.33 kg
Prestressing Force at transfer	$P_o = K_1 \times P_i$		=	117,907.12 kg	94,325.70 kg
Effective Prestressing Force	$P_e = K_2 \times P_i$		=	102,186.17 kg	81,748.94 kg

ULTIMATE LOAD CAPACITY

Ratio of ps reinforcement, ρp	=	0.0018780	
Stress in ps reinforcement, f_{ps}	=	17,553.50 kg/cm^2	
Depth of eq. rectangular sb., a	=	7.2720 cm.	
Prestressing steel index, ω_p	=	0.08	O.K.

FLEXURAL DESIGN

Ultimate moment, M_u	=	59,558.39 kg-m
Cracking moment, M_{cr}	=	41,168.90 kg-m
Flexural srength, M_n	=	62,633.17 kg-m
$\phi M_n \geq M_u$		O.K.
$\phi M_n \geq 1.2 M_{cr}$		O.K.

HOLLOW CORE SLAB DESIGN

[4] SERVICE LOAD STRESSES

STRESSES (kg/cm^2)	Support at release		Mid span at release		Midspan at Service load		
	P=P$_s$ = 94,326		P=P$_s$ = 117,907		P=P$_f$ = 102,186	kg.	
	f$_b$	f$_t$	f$_b$	f$_t$	f$_b$	f$_t$	f$_{tr}$
P/A	40.68	40.68	50.86	50.86	44.07	44.07	
eP/Z	70.29	-70.27	87.86	-87.84	76.15	-76.13	
M$_{d}$/Z	-0.96	0.96	-45.78	45.77	-45.78	45.77	
M$_{sd}$/Z					-21.03	21.02	
M$_{ad}$/Z					-14.31	0.11	10.80
M$_{ll}$/Z					-64.41	31.22	48.58
Stresses	110.02	-28.63	92.94	8.78	-25.31	66.06	59.38
Limiting Stresses	0.7f'c	-2√f'c	0.7f'c	0.7f'c	-2√f'c	0.45f'c	0.6f'c
	196.00	-33.47	196.00	196.00	-40.00	180.00	240.00
	O.K.	O.K.	O.K.	O.K.	O.K.	O.K.	O.K.

Overall member length: l$_p$	=	12	m.	M$_{ultimate}$ = 209.758 kg-m
Strand transfer length: l$_t$	50d$_b$ =	6.35	cm	debonded = 2 strands

[5] CAMBER & DEFLECTION

Mid Span moment M = P$_r$e	1.922E+06 kg-cm	E$_1$ =	265,659	kg/cm^2	I$_1$ = 437,581	cm^4
CAMBER $\delta_{camber} = \frac{ML^2}{8EI}$	3.35E+11 /EI	E$_2$ =	317,523	kg/cm^2	I$_2$ = 437,581	cm^4
DEFLECTION $\delta_{deflect} = \frac{5WL^4}{384EI}$	2.70E+08 w/EI	E$_3$ =	317,523	kg/cm^2	I$_3$ = 800,235	cm^4

		Release (cm.)	Multiplier	Erection (cm.)	Multiplier	Final (cm.)
PRESTRESS CAMBER		2.881	1.80	5.186	2.20	6.339
Slab weight, Wdl	556.44	-1.292	1.85	-2.391	2.40	-3.102
		1.589		2.795		3.237
Topping weight, W$_{sdl}$	255.56			-0.497	2.30	-1.142
SDL, W$_{adl}$	240.00			-0.255	3.00	-0.765
Live Load, W$_{ll}$	1,080.00			2.044		-1.148

CAMBER 0.182

Maximum permissible computed deflections: L/360 -3.333

Remark: + is upward

+ is downward

HOLLOW CORE SLAB DESIGN

[6] SHEAR DESIGN

At h/2 from support.

Ultimate shear force, V_u	=	19,066.96	kg
Ultimate shear stress, V_u	=	12.80	kg/cm^2
Compressive stress in concrete at centroid, f_{pc}	=	44.07	
Ultimate Shear strength, ϕV_c	=	47,389.89 kg > 19,066.96 kg	O.K.

SHEAR RESISTING DESIGN

	Ultimate Shear strength, ϕV_c =	47,389.89 kg	
Exceed Shear force	$V'_u = 0.85 V_c - V_u$ =	0.00 kg	
	Filling	0	Hollow core to increase b_w
	Filled b_w	0	cm.
	Filling		cm. long .

TRANSPORTATION AND INSTALLATION PLANNING

HOLLOW CORE WALL PANEL DESIGN
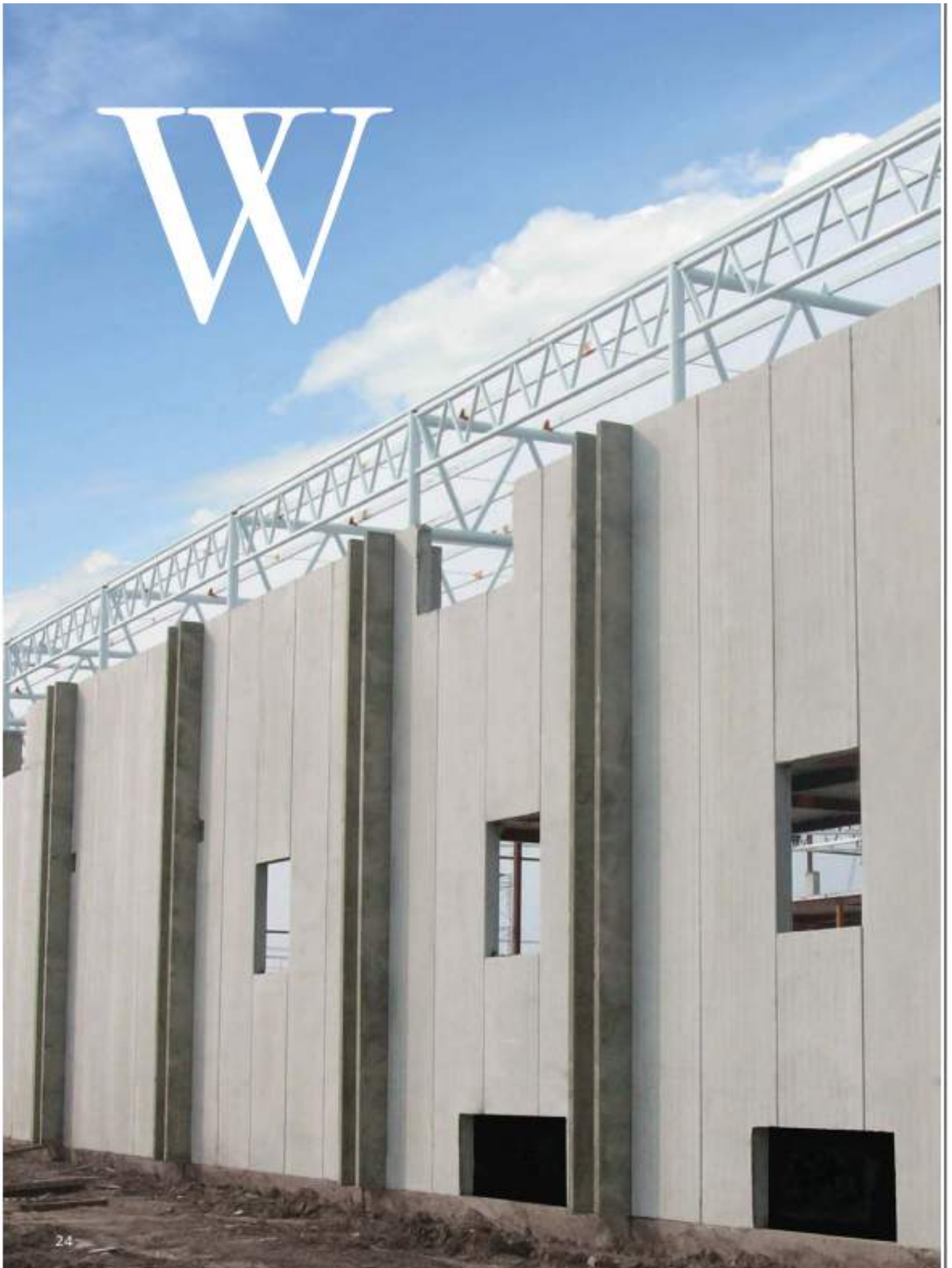
HOLLOW CORE WALL PANEL INSTALLATION

WALL PANEL TEXTURE

CONCRETE FINISH

ACID-ETCHED

POLISHED

SAND-BLASTED RIB

EXPOSED AGGREGATE

BUSH-HAMMERED RIB

POLISHED RIB

TERRAZZO RIB SURFACE WALL PANEL
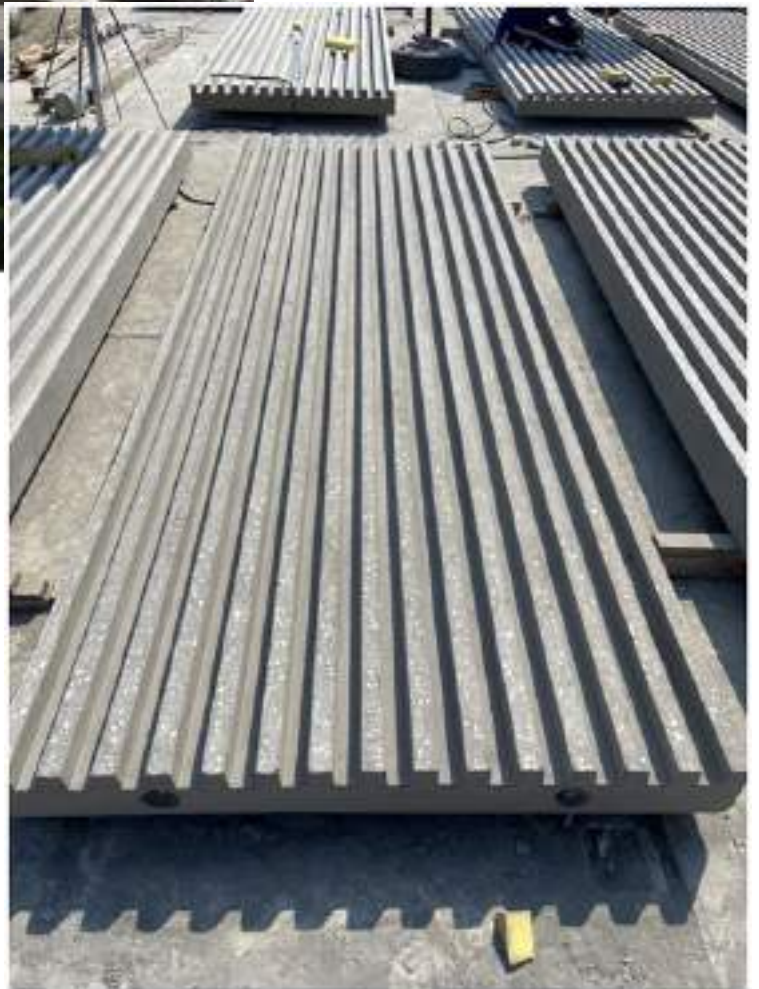
BUSH
HAMMERED
RIB

POLISHED
RIB

HOLLOW CORE WALL PANEL CONNECTION DESIGN

Hollow core wall panel - vertical joint and
connection design

ISOMETRIC
VCON Wall Panel Vertical Joint

Mortar finishes

Gasket seal as needed

Sealant

Steel plate welded
with building structure
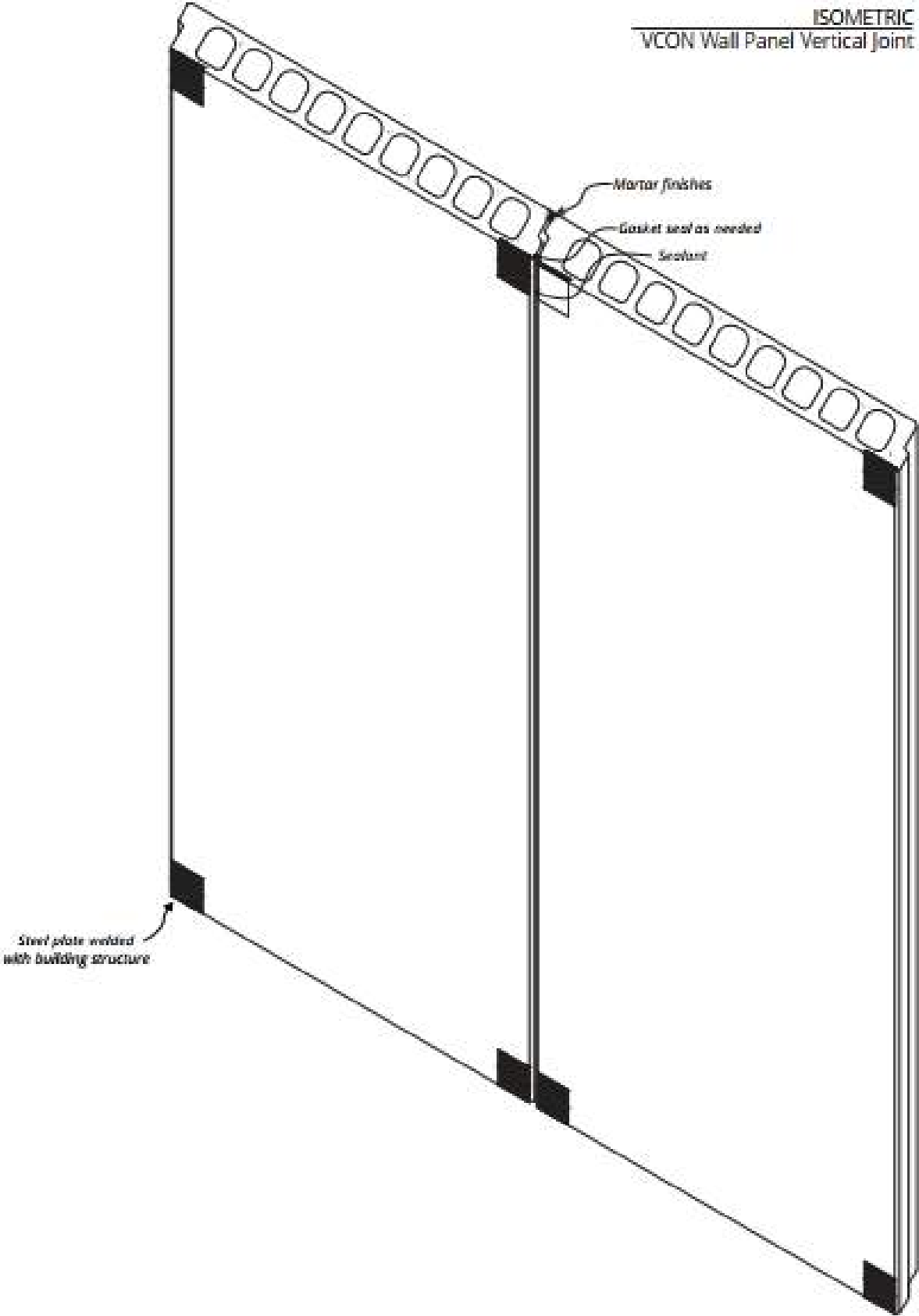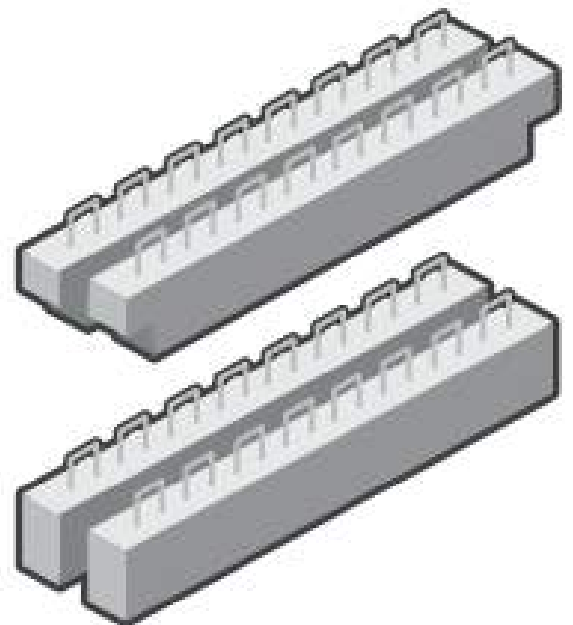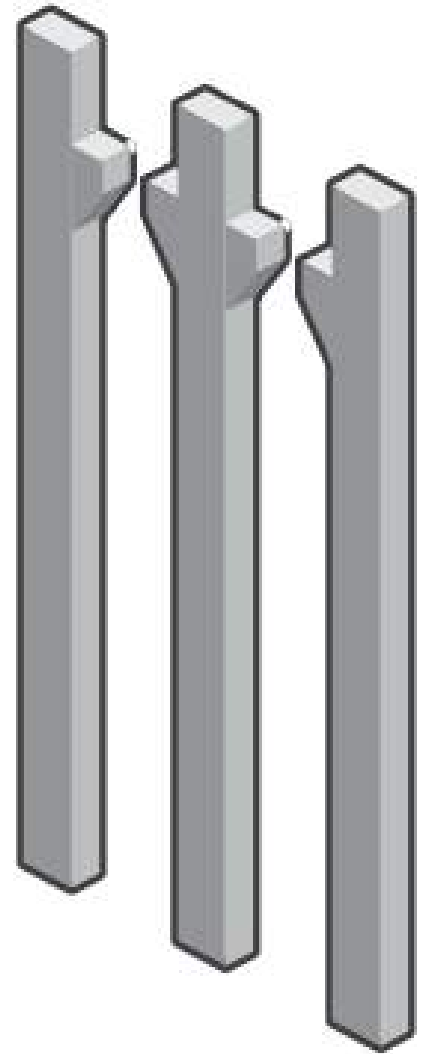
P

PRECAST COLUMN AND BEAM

Wide range of techinical possibilities, extremely durable.

GFRC
Glass Fiber Reinforced Concrete

EMQUATIER MALL
SOLID PRECAST With GRFC SURFACE

SIAM PREMIUM OUTLET
GRFC SURFACE With GALVANIZED STEEL FRAME

SIAM PREMIUM OUTLET
GRFC SURFACE With GALVANIZED STEEL FRAME

DESIGN STANDARD